arXiv:1304.4911v1 [cond-mat.mtrl-sci] 17 Apr 2013

Predicted strain-induced isosymmetric ferri-to-ferroelectric transition with large piezoelectricity

Gaoyang Gou[1, *] and James M. Rondinelli[2, †]
[1] *Frontier Institute of Science & Technology, Xi' an Jiaotong University, Xi' an 710049, China*
[2] *Department of Materials Science & Engineering, Drexel University, Philadelphia, PA 19104, USA*

(Dated: April 18, 2013)

We identify a first-order, isosymmetric, transition between a ferrielectric (FiE) and ferroelectric (FE) state in A-site ordered LaScO$_3$/BiScO$_3$ and LaInO$_3$/BiInO$_3$ superlattices. This unusual electrical analogue to the pervasive ferrimagnetic state in magnetic oxides relies on a geometric field imposed by octahedral rotations and enabled by cation ordering—it decouples the local electric dipoles on the cationic sublattices and directs their cooperative alignment. Epitaxial strains less than 2% are predicted to be sufficient to transverse the phase boundary, across which we capture a ∼5X increase in electric polarization. We describe the electromechanical responses and show that at fixed composition the FiE-to-FE transition may be superior to the polarization reversal found in Pb-based perovskite oxide solid-solutions, enabling piezoelectric technologies under extreme conditions.

PACS numbers: 77.84.-s, 81.05.Zx, 71.15.Mb, 68.55.-a

Introduction.—Ferroic materials are characterized by the loss of spacial and/or temporal symmetries. Independent of the microscopic ordering, symmetry removal provides for functional responses that couple multiple degrees of freedom, activating new physical tensor properties. Perovskite ABO_3 oxides with broken space inversion symmetry often exhibit a spontaneous and switchable electric polarization: Ferroelectric (FE) ordering induces an alignment of local electric dipoles, in analogy to the cooperative ordering of local magnetic moments in ferromagnetic crystals without time-reversal symmetry. Much rarer in crystalline materials with an electric polarization, however, is the appearance of a *ferrielectric* (FiE) state, *vis-á-vis* ferrimagnetism, where local electric dipoles of different magnitude are anti-aligned to yield a net nonzero electric polarization [1–4]. The underlying reason being that the long-range Coulomb forces in oxide-based dielectrics favor the cooperative alignment of all electric dipoles in the crystal [5] through cation displacements that occur against an oxygen ligand framework [6].

The recent discovery of a class of hybrid improper ferroelectrics (HIF) [7, 8], whereby the electric polarization originates from a non-zero cancellation of electric layer polarizations, or unequal local electric dipoles moments, $\vec{p}$, among three cation sublattices is a realization of the FiE state [9]. In cation ordered $(A, A')B_2O_6$ oxides, equivalently 1/1 superlattices constructed interleaving ABO$_3$/A$'$BO$_3$ blocks along [001], the layer dipoles are restricted by symmetry to be directed along the pseudocubic ⟨110⟩ directions. At present, all known examples of this type are found to have two of the three possible cation-sublattice dipoles aligned with each other, *e.g.* [110], while the third is anti-parallel to the others, [$\bar{1}$10] [10]. A rotocrystalline anisotropy stabilizes the FiE state, because the electric dipoles of the A-site sublattice are constrained by the "sense" of the orthorhombic $a^-a^-c^+$ BO_6 rotations [11] in Glazer notation [12]. The electric polarizations of each sublattice, therefore, may be tuned independently—the A and B cation sublattice polarizations rely on the geometric field imposed by the rotations, which can decouple the electrostatic alignment of the layer dipoles. Can a suitable "field" convert the FiE state directly into a FE state without passing through a paraelectric intermediate? If answered in the affirmative, then a rotation-enabled route to achieve a significant polarization enhancement *and* large piezoelectric response in synthetically ordered perovskites would be realized.

In this Letter, we use first-principles density functional calculations to demonstrate that the *polarization switching* between a FiE and FE phases in the $(A, A')B_2O_6$ perovskites is accessible with substrate-induced epitaxial strain. Specifically, we uncover a first-order isosymmetric phase transition and evaluate the feasibility of the FiE-to-FE transition through a minimum energy path (MEP) trajectory. We find enhanced electromechanical responses when passing through the metastable intermediate structure, which resemble and are comparable to the the composition-dependent morphotropic phase boundaries (MPB) in solid-solution PbZr$_{1-x}$Ti$_x$O$_3$ [13, 14], where a large piezoelectric response is driven by rotation of polarization along an easy *rotation path* between *polar* rhombohedral and tetragonal phases through a monoclinic intermediate [15, 16]. Lastly, we describe how the transition manifests as an effective MPB without requiring a change in octahedral rotation sense. It has the practical advantage of occurring within a single phase material without a change in symmetry and at integral stoichiometry—features useful for facile switching and mitigating piezoelectric fatigue [17].

Models and Simulation Details.—We select ultra-short LaMO$_3$/BiMO$_3$ perovskite superlattices, with trivalent cations M = Ga, Sc and In, respectively, to guarantee the insulating behavior required to sustain an electric polarization. The $6s^2$ stereochemical lone pair of Bi pro-

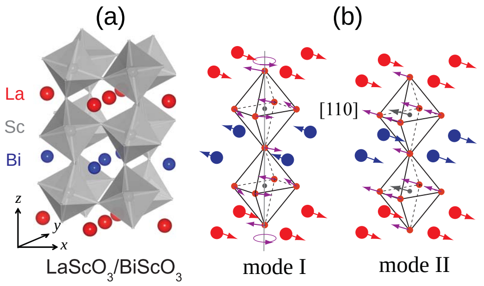

FIG. 1. (Color online) (a) The *Pmma* paraelectric structure of the LaScO$_3$/BiScO$_3$ superlattice with the $a^-a^-c^0$ rotation pattern (a). The displacement patterns of the corresponding soft phonon modes (b): $\omega_{\rm I}$ with *anti-parallel* La-O/Bi-O in-plane displacements (left), and $\omega_{\rm II}$ with *parallel* La-O/Bi-O in-plane displacements (right).

motes structural distortions and enhanced polarizability [18]. Lastly, each bulk $A^{3+}M^{3+}O_3$ oxide forming the superlattices exhibits the targeted orthorhombic $a^-a^-c^+$ octahedral rotation pattern (Fig. S1 of Ref. 19) conducive to HIF [11].

Our density functional theory (DFT) calculations are performed with the QUANTUM ESPRESSO code [20], with optimized nonlocal norm-conserving [21] pseudopotentials, a 60 Ry plane-wave cutoff, and the PBEsol functional [23]. The Brillouin zone (BZ) integrations use a 8×8×8 Monkhorst-Pack k-point grid [22]. Low-energy phases are obtained by performing complete structural relaxations on soft-mode generated structures until the Hellmann-Feynman forces on the atoms are less than 0.1 meV Å^{-1}. For the strained films, the out-of-plane lattice constant is relaxed until the stresses are less than 0.1 kbar. The electronic contribution to the polarization is calculated following the Berry phase formalism [26]. The minimum energy path (MEP) between the stable phases is simulated using the nudged elastic band (NEB) method [27].

Ground State Structures.—We find the lowest energy structures by computing the phonons in the BZ of the parent $P4/mmm$ phase, *i.e.*, the distortion-free structure obtained from A/A' cation ordering along [001]. We find four unstable vibrational phonons in each superlattice: They are characterized as either in-phase (irreducible representation M_3^+ relative to $Pm\bar{3}m$) or out-of-phase rotations (R_4^+) of MO_6 octahedra, or polar inversion symmetry lifting cation displacements along [110] (Γ_4^-) and [001] against the oxygen framework, respectively [19]. For all superlattices, the most unstable modes are out-of-phase rotations, $a^-a^-c^0$, with the mode-frequency of the gallate smaller than the scandate or indiumate due to the larger tolerance factor of the former [9].

We next freeze-in each soft mode into the $P4/mmm$ superlattices followed by full structural relaxations to obtain lower symmetry distorted phases. For each superlattice, we find a stable non-polar *Pmma* phase with the $a^-a^-c^0$ rotation [Fig. 1(a)]. We now take this as the relevant paraelectric phase for which transitions between lower-symmetry polar phases could occur. We find two unstable vibrational modes in the *Pmma* superlattices (Table SII in Ref. 19): $\omega_{\rm I}$ and $\omega_{\rm II}$ correspond to atomic displacement vectors that are either a combination of in-phase octahedral rotations and anti-parallel A cation displacements, or cooperative polar cation displacements moving in the direction opposite of the oxygen anions [Fig. 1(b)], respectively.

TABLE I. The relative energetic stability (in meV/f.u.) with respect to the ground state $Pmc2_1$ (phase I) structure for various low-energy phases specified by Glazer tilt; subscripts indicate the direction of the electric polarization following the convention in Ref 28. The average tolerance factor ($\bar{\tau}$) for each perovskite superlattice is given in parentheses.

	$Pmma$	$[Pmc2_1]_{\rm I}$	$[Pmc2_1]_{\rm II}$	Pc
System / Rotation	$a_0^-a_0^-c_0^0$	$a_+^-a_+^-c_0^+$	$a_+^-a_+^-c_0^+$	$a_+^-a_+^-c_+^-$
LaInO$_3$/BiInO$_3$ (0.87)	437	0	109	179
LaScO$_3$/BiScO$_3$ (0.89)	338	0	57	170
LaGaO$_3$/BiGaO$_3$ (0.94)	97	0	–	–

We now combine the *Pmma* structures with the displacement vectors for $\omega_{\rm I}$ and $\omega_{\rm II}$. The symmetry of the superlattices all reduce to the *same* polar space group $Pmc2_1$ (no. 26), where the polar axis is along the pseudocubic [110] direction, despite the physical difference in the displacement vector. Hereafter, we distinguish between the two symmetry equivalent $Pmc2_1$ phases as (I) or (II), appended as a subscript to the space group label. After performing a full structural relaxation, we find that the $[Pmc2_1]_{\rm I}$ phase is the global ground state for all superlattices (Table I). Except for LaGaO$_3$/BiGaO$_3$, $[Pmc2_1]_{\rm II}$ is the next lowest energy phase, *e.g.*, 57 meV per formula unit (f.u.) higher in energy than $[Pmc2_1]_{\rm I}$ in LaScO$_3$/BiScO$_3$ [29]. The small energy barrier suggests transition between the two $Pmc2_1$ phases may be achieved by thin film epitaxy.

To understand the microscopic origin of the energy difference between the two isosymmetric $Pmc2_1$ phases, we focus on the LaScO$_3$/BiScO$_3$ superlattice, and examine its local atomic structures in more detail. Fig. 2(a) and (b) shows both polar phases projected along the [100] and [011] directions. Each possesses the same $a^-a^-c^+$ rotations, but *different cation displacement patterns*, which become readily apparent in the layer-resolved electric polarizations [Fig. 2(c)]. $[Pmc2_1]_{\rm I}$ is described by a ferri-electric state, whereby a non-cancellation of anti-aligned layer electric dipoles from the alternating LaO or BiO planes produces a overall non-zero electric polarization. In $[Pmc2_1]_{\rm II}$, $\vec{p}_{\rm BiO}$ switches from anti-parallel to parallel alignment with $\vec{p}_{\rm LaO}$. All cations displace in the same direction, as a conventional ferroelectric, to give a >5X polarization enhancement.

Phase I is obtained by condensation of the ω_I soft mode,

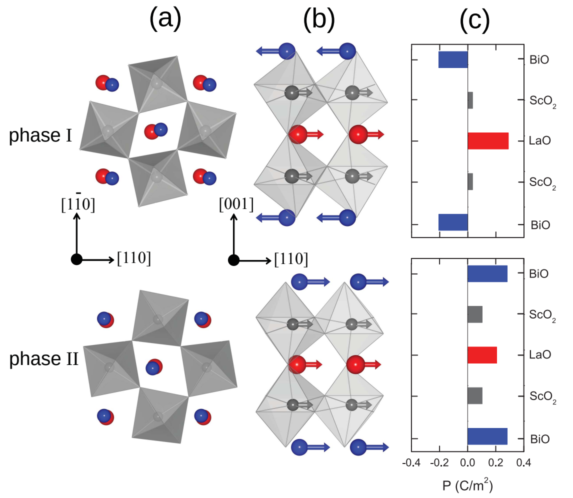

FIG. 2. (Color online) Atomic structures of the two isosymmetric polar ground states ($a_+^-a_+^-c_0^+$) with $Pmc2_1$ symmetry: phase I (upper) and phase II (lower). Both top view (a) and side view (b) are shown to emphasize cation displacement directions (arrows). (c) Layer-revolved polarization $\vec{p}_{layer} = \Omega^{-1}\sum_i u_i Z_i^*$, where Ω is the cell volume, u_i is the i cation displacement and Z_i^* is the Born effective charge. Phase I is *ferrielectric* (total polarization, $P = 0.12$ C/m^2) with anti-parallel $\vec{p}_{\mathrm{LaO}}$ and $\vec{p}_{\mathrm{BiO}}$, while Phase II is a normal *ferroelectric* ($P = 0.63$ C/m^2), where both $\vec{p}_{\mathrm{LaO}}$ and $\vec{p}_{\mathrm{BiO}}$ are oriented in the same direction.

and the polar displacements are stabilized from a combination of the $a^-a^-c^0$ and $a^0a^0c^+$ octahedral rotations (Fig. S1). Interestingly, the extraordinary large energy gain between polar and paraelectric states of $LaScO_3/BiScO_3$ (338 vs. 48 meV/f.u. as in $BaTiO_3$ [30]) indicates the polarization should persist to high temperatures, similar to what found in other HIF oxides [31]. The polarization in phase II arises from the polar instability ω_{II} in $Pmma$, where cooperative displacement of *all* cations occur in the same direction and are opposite to that of the oxygen atoms, as found in proper ferroelectrics, *e.g.*, $BaTiO_3$. Moreover, phase II has a *suppressed* in-phase rotation amplitude compared to phase I (Fig. S2) in the presence of a greater electric polarization, indicating the trilinear coupling term connecting the octahedral rotations to the polarization contributes less to the ground state [8, 9].

Strain-induced FiE-to-FE Transition.—We calculate the evolution of the total energy for the $Pmc2_1$ phases with respect to applied epitaxial strain [Fig. 3(a)]. We find in $LaScO_3/BiScO_3$, the transition from $[Pmc2_1]_{\mathrm{I}}$ to $[Pmc2_1]_{\mathrm{II}}$ occurs approximately at 1.0% tensile strain, accompanied by an abrupt change in the overall polarization [Fig. 3(b)]. The transition between the $Pmc2_1$ phases is first-order and isosymmetric [32]. Critically, no octahedral rotation-reversal is necessary; only a reduction in amplitude is required, indicating polarization reversal between the two states should be experimentally simpler to achieve than in other HIF.[8] (See Fig. S2 for detailed structural analysis.) The ferri-to-ferroelectric transition also occurs in the indium superlattice, albeit at a larger strain ($\simeq$2.0%), yet it is not found in the gallium compound [19]. The larger tolerance factor for the $LaGaO_3/BiGaO_3$ reduces the energy gain between $Pmma$ and $[Pmc2_1]_{\mathrm{I}}$ (Table I), and makes the $[Pmc2_1]_{\mathrm{II}}$ phase unstable. In the remainder of this Letter, we focus on the strained $LaScO_3/BiScO_3$ with an emphasis on response property enhancement near the FiE-to-FE transition.

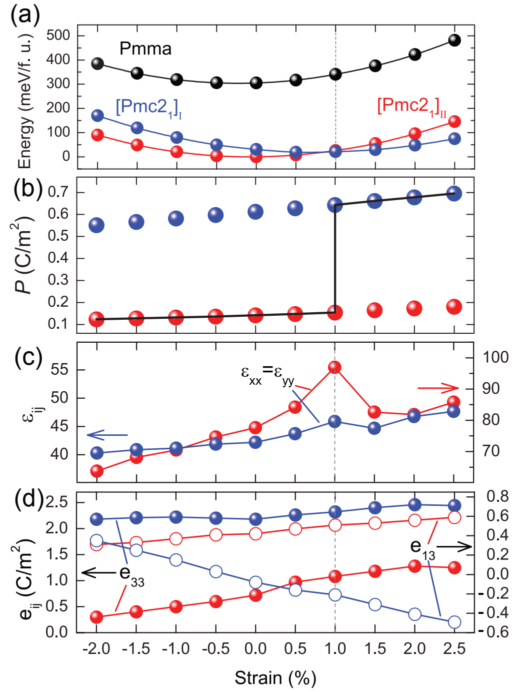

FIG. 3. (Color online) Strain-dependent phase stability and electronic properties of $LaScO_3/BiScO_3$: (a) total energies for the paraelectric and polar structures, (b) total polarization [the bold black line transverses the polarization of the lowest energy structures in (a)], (c) static dieletric tensor ϵ_{ij} (ϵ_{xx}=ϵ_{yy}, filled circles), and (d) the piezoelectric stress constants e_{ij} (e_{33}, filled circles; e_{31} empty circles) for $Pmc2_1$ phase I (red) and II (blue). The isosymmetric transition occurs at 1.0% tensile strain (broken lines).

The evolution of the response functions, including the dielectric permittivity and piezoelectric response, as a function of strain are computed at the DFT-level [33]. Fig. 3(c) shows that the in-plane dielectric susceptibility ε_{xx} and ε_{yy} are maximum at the FiE-to-FE transition at 1.0 % tensile strain in both $Pmc2_1$ phases, consistent with a first-order transition at this critical strain [34]. In Fig. 3(d), we also plot piezoelectric stress constants e_{33} and e_{13}, which evolve smoothly with respect to strain. The non-zero piezoelectric strain coefficients d_{ij} for the FiE and FE phases at 1.0% strain are also reported in Table II. Compared to proper FE perovskites, each polar $LaScO_3/BiScO_3$ displays a modest piezoelectric response. In polar $Pmc2_1$ state where the polarization is induced

TABLE II. Calculated non-zero piezoelectric stress constants e_{ij} (C/m^2) and piezoelectric strain coefficients d_{ij} (pC/N) for each phase of LaScO$_3$/BiScO$_3$ at 1.0% tensile strain.

	$[Pmc2_1]_{\rm I}$		$[Pmc2_1]_{\rm II}$	
index (ij)	e_{ij}	d_{ij}	e_{ij}	d_{ij}
31	0.50	-1.05	-0.19	-6.16
32	1.05	2.33	0.77	0.91
33	1.34	5.23	2.45	15.66
24	0.93	14.57	1.03	17.96
15	1.10	14.30	1.23	21.61

by octahedral rotations, the dominant strain-rotation coupling will mitigate the effective coupling between strain and polar displacements [35, 36], making hybrid-improper ferroelectric oxides weak piezoelectrics for transducer applications [31]. Despite the small piezoelectric moduli found in the individual $[Pmc2_1]_{\rm I}$ and $[Pmc2_1]_{\rm II}$ phases, one should also consider enhancements due to the FiE-to-FE transition in describing the macroscopic functionality.

Piezoelectricity at the FiE-to-FE Transition.—To evaluate the consequence of the FiE-to-FE transition on piezoelectricity, we first map out the energy landscape in the vicinity of the low energy phases (Fig. 4). The two-dimensional energy contours at 1.0% strain for LaScO$_3$/BiScO$_3$ are computed by varying the amplitude of the eigenvectors of the unstable *Pmma* phonons. We find that the FiE $[Pmc2_1]_{\rm I}$ and FE $[Pmc2_1]_{\rm II}$ phases are located at minima near the major axes and are separated by a energy barrier.

We estimate the feasibility of the FiE-to-FE transition by calculating the energy barrier separating the two stable structures along a MEP obtained from the NEB method [Fig. 4(b)]. We find a small, nearly strain-independent 106 meV/f.u. barrier separating the phases [37], and comparable to the polarization rotation barrier in piezoelectric PbTiO$_3$ [38], suggesting the FiE-to-FE transition should be energetically accessible [39].

We emphasize that the polarization rotation at the $[Pmc2_1]_{\rm I} \rightarrow [Pmc2_1]_{\rm II}$ transition [Fig. 5(a)] along the MEP is due to a change in direction of Bi displacements along [110] direction in (001) planes above and below the ScO$_2$ layers (Fig. 2). $\vec{p}_{\rm BiO}$ switches from anti-parallel to parallel alignment with $\vec{p}_{\rm LaO}$ along the polar axis by decreasing its amplitude in the (001) plane until reaching the saddle point in the energy landscape [Fig. 5(b)]. Here, a nearly random distribution of the Bi lone pairs within the planes emerges [Fig. 5(d)], and we find a transformation of BiO$_8$ polyhedra into highly distorted BiO$_4$ tetrahedra with enhanced Bi^{3+} electron lone pair activity in $[Pmc2_1]_{\rm II}$ [Fig. S4 and Fig. S5]. After the saddle point, $\vec{p}_{\rm BiO}$ continues to increase while $\vec{p}_{\rm LaO}$ remains nearly unchanged.

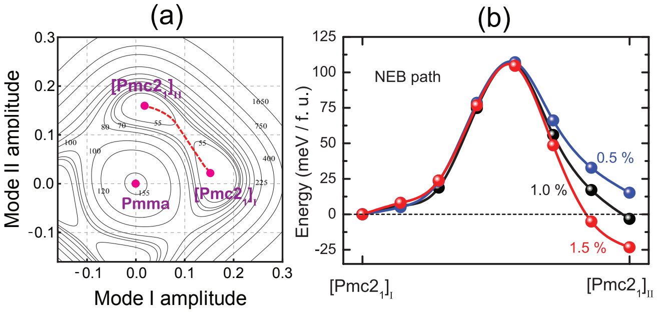

FIG. 4. (Color online) The calculated two-dimensional energy surface contours for LaScO$_3$/BiScO$_3$ with respect to the soft phonons of *Pmma* (a); energy contours in meV. The MEP between two polar states for LaScO$_3$/BiScO$_3$ under tensile strain (b) reveals a small energy barrier.

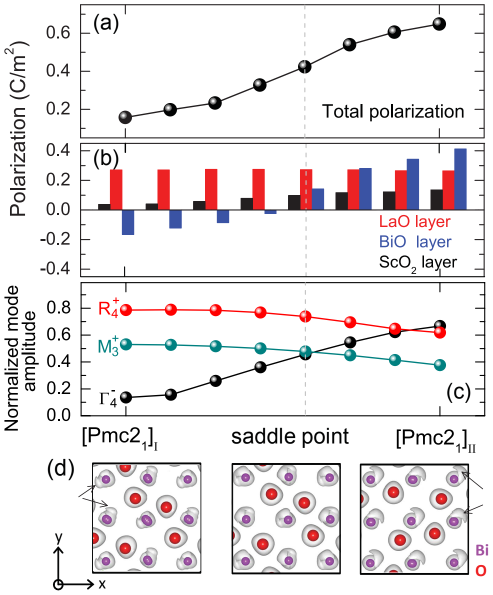

FIG. 5. (Color online) The calculated (a) total polarization, (b) layer-revolved polarizations and (c) major crystallographic mode amplitudes for each image along the MEP connecting phase I and II in LaScO$_3$/BiScO$_3$ at 1.0 % strain. The position of the saddle point along the MEP is shown as dashed line. Electronic-localization-function (ELF) surfaces within the BiO layer for phase I, the intermediate structure at the saddle point, and phase II (d). Across the FiE-to-Fe transition, the Bi electron lone pair (small lobe, arrowed) alignment reverses.

The change in mode amplitudes along the MEP is dominated by a large enhancement of Γ_4^- polar displacement (>5X), with the moderate change in octahedral rotations [$\simeq$25%, Fig. 5(c)]. This structure evolution indicates the lattice strain–polarization coupling can exceed the strain–rotation interactions across the FiE-to-FE transition, despite reduced coupling in each individual phase. Because the polarization remains finite – the FiE state is directly converted into FE state without passing through any paraelectric intermediate – the changes in polyhedral coordination at the transition can produce a large induced electric polarization upon application of a stress. The

FiE→FE transition occurs through an easy *polarization switching path* with a large polarization enhancement and strong strain–polarization coupling. Indeed, the piezoelectric moduli are enhanced from 3-6X across the transition (Table II), which is qualitatively similar to conventional MPB oxides [14], yet occurs at fixed composition.

Outlook & Summary.—We used first-principles calculations combined with group theoretical studies to uncover a first-order, isosymmetric, structural transition between a FiE and FE state in artificial A-site ordered perovskite superlattices. For $LaScO_3/BiScO_3$, we predict 1% tensile epitaxial strain is sufficient to induce the FiE-to-FE transition with electrical features that could enable rational technology design: A single phase material with a two-state polarization enabled by strong strain-polarization coupling, and simultaneously large piezoelectric responses driven by reversal of cation displacements without changes to the sense of octahedral rotations or crystallographic symmetry—features absent in conventional ferroelectric ceramics with MPB. Second, owing to the extraordinary large energy gain between the polar and paraelectric states, the FE-to-FiE transition should persist up to high temperature ($T > 500°C$), where Pb-based piezoelectrics responses are impaired. Finally, ferrielectric materials should exhibit similar electrical switching behavior as antiferroelectrics, *e.g.*, double hysteresis loops that improve energy density capacities [40], yet with the advantage of polarization reversal at much lower fields, enabling practical integration for energy harvesting devices.

G.Y.G. was supported by the NBR Program of China (2012CB619401), NSFC (11204230) and acknowledges computational support from NSCC. G.Y.G. thanks Prof. Chao Wu and Mr. Jing Shi for assistance in preparing this manuscript. J.M.R. was supported by ARO (W911NF-12-1-0133) and thanks C.J. Fennie and A.T. Mulder for insightful discussions.

---

* gougaoyang@mail.xjtu.edu.cn
† jrondinelli@coe.drexel.edu

[1] L. E. Cross, Philosophical Magazine **1**, 76 (1956).
[2] C. F. Pulvari, Phys. Rev. **120**, 1670 (1960).
[3] I. Suzuki *et al.*, J. Phys. Soc. Jpn. **45**, 1302 (1978).
[4] A. K. Tagantsev, JETP Lett. **45**, 447 (1987).
[5] W. Cochran, Phys. Rev. Lett. **3**, 412 (1959).
[6] R. E. Cohen, Nature **358**, 136 (1992).
[7] E. Bousquet *et al.*, Nature **452**, 732 (2008).
[8] N. A. Benedek *et al.*, Phys. Rev. Lett. **106**, 107204 (2011).
[9] A. T. Mulder *et al.*, ArXiv e-prints (2012), 1205.5526.
[10] N. A. Benedek *et al.*, J. Solid State Chem. **195**, 11 (2012).
[11] J. M. Rondinelli *et al.*, Adv. Mater. **24**, 1961 (2012).
[12] A. M. Glazer, Acta Cryst. B **28**, 3384 (1972).
[13] R. Guo *et al.*, Phys. Rev. Lett. **84**, 5423 (2000).
[14] H. Fu *et al.*, Nature **403**, 281 (2000).
[15] B. Noheda *et al.*, Phys. Rev. Lett. **86**, 3891 (2001).
[16] I. Grinberg *et al.*, Nature **419**, 909 (2002).
[17] P. Chen *et al.*, New Journal of Physics **14**, 013034 (2012).
[18] R. Seshadri *et al.*, Chem. Mater. **13**, 2892 (2001).
[19] See supplementary material at `http://link.aps.org/supplemental/XYZ` for details.
[20] P. Giannozzi *et al.*, J. Phys.: Condens. Matter **21**, 395502 (2009).
[21] A. M. Rappe *et al.*, Phys. Rev. B **41**, 1227 (1990); N. J. Ramer *et al.*, Phys. Rev. B **59**, 12471 (1999).
[22] H. J. Monkhorst *et al.*, Phys. Rev. B **13**, 5188 (1976).
[23] J. P. Perdew *et al.*, Phys. Rev. Lett. **100**, 136406 (2008).
[24] S. Baroni *et al.*, Rev. Mod. Phys. **73**, 515 (2001).
[25] X. Gonze, Phys. Rev. A **52**, 1096 (1995).
[26] R. D. King-Smith *et al.*, Phys. Rev. B **47**, 1651 (1993).
[27] G. Henkelman *et al.*, J. Chem. Phys. **113**, 9901 (2000); J. Chem. Phys. **113**, 9978 (2000).
[28] H. T. Stokes *et al.*, Acta Cryst. B **58**, 934 (2002).
[29] $LaScO_3/BiScO_3$ and $LaInO_3/BiInO_3$ also possess a low energy polar Pc structure with a polarization component along [001]; however, the structures are more than 170 meV/f.u. higher energy and likely inaccessible via substrate-induced epitaxial strain at room-temperature. Therefore, we do not consider it further.
[30] S. Sanna *et al.*, Phys. Rev. B **83**, 054112 (2011).
[31] J. López-Pérez *et al.*, Phys. Rev. B **84**, 075121 (2011).
[32] J. M. Rondinelli *et al.*, Phys. Rev. Lett. **106**, 235502 (2011).
[33] X. Wu *et al.*, Phys. Rev. B **72**, 035105 (2005).
[34] Z. Wu *et al.*, Phys. Rev. Lett. **95**, 037601 (2005).
[35] R. D. King-Smith *et al.*, Phys. Rev. B **49**, 5828 (1994).
[36] P. Aguado-Puente *et al.*, Phys. Rev. Lett. **107**, 217601 (2011).
[37] The height of the energy barrier is also consistent with that obtained from the energy contour plot in Fig. 4.
[38] J. Hong *et al.*, Phys. Rev. B **84**, 115107 (2011).
[39] The experimental switching path will also depend on extrinsic factors, including the coexistence of two monodomains, domain-wall formation, and coalescence, cf. W. J. Merz, Phys. Rev. **95**, 690 (1954). The calculated energy barrier of the monodomain crystal provides a reasonable estimate of the easy switching path within the strained $LaScO_3/BiScO_3$ superlattice.
[40] L. Zhu *et al.*, Macromolecules **45**, 2937 (2012).